European Journal of Pharmaceutics and Biopharmaceutics xxx (2013) xxx–xxx

Contents lists available at ScienceDirect

European Journal of Pharmaceutics and Biopharmaceutics

journal homepage: www.elsevier.com/locate/ejpb

Research paper

Transport mechanism of doxorubicin loaded chitosan based nanogels across intestinal epithelium

Chao Feng [a], Guohui Sun [a], Zhiguo Wang [b], Xiaojie Cheng [a], Hyunjin Park [c], Dongsu Cha [c], Ming Kong [a,*,1], Xiguang Chen [a,*,1]

[a] College of Marine Life Science, Ocean University of China, Qingdao, China
[b] Department of Plastic Surgery, The Affiliated Hospital of Medical College Qingdao University, Qingdao, China
[c] Graduate School Biotechnology, Korea University, Seoul, South Korea

ARTICLE INFO

Article history:
Received 4 October 2013
Accepted in revised form 28 November 2013
Available online xxxx

Keywords:
Carboxymethyl chitosan
Nanogels
Transport pathway
Doxorubicin hydrochloride
Drug permeability
Oral delivery

ABSTRACT

Chitosan/carboxymethyl chitosan nanogels (CS/CMCS-NGs) could enhance the oral bioavailability of doxorubicin hydrochloride (DOX). To identify the mechanisms that support this recent observation, different transport pathways of CS/CMCS-NGs through the small intestine were studied in this work. Transcellular mechanisms were investigated in the presence of different inhibitors of protein-mediated endocytosis. A reduction of 52.32 ± 18% of drug transport was found when clathrin-mediated endocytosis was inhibited, which demonstrated that clathrin-mediated endocytosis played an important role in the transcellular transport of DOX:CS/CMCS-NGs. The paracellular transport results showed that CMCS in NGs could produce a transient and reversible enhancement of paracellular permeability by depriving Ca^{2+} from adherens junctions, whose efficacy as an absorption enhancer was about 1.7–3.3 folds higher than CS in NGs in GI tract. Finally, *in vivo* experiment showed that the transport capacity of DOX:CS/CMCS-NGs was significantly inhibited by extra added Ca^{2+}, which confirmed that the higher capacity to binding Ca^{2+} of CS/CMCS-NGs was beneficial for transport of DOX.

1. Introduction

In the current regimen of chemotherapy, the anticancer drugs are administered through i.v. injection or infusion. Although it is effective for cancer therapy, the side effect due to the direct delivery of high concentration anticancer-drug to bloodstream and the inconveniences during chemotherapy compromise its clinical treatment efficacy [1,2]. Oral administration of anticancer drugs is a viable alternative to intravenous administration, since it can maintain an optimum blood drug concentration and improves convenience and compliance of patients [3,4]. Nevertheless, most anticancer drugs especially those with excellent anticancer effects such as doxorubicin hydrochloride (DOX) and Taxanes (paclitaxel and docetaxel) are not orally bioavailable owing to inadequate transport throughout the intestinal epithelium [5].

To improve oral bioavailability of anticancer drugs, Chitosan based nanogels (CS/CMCS-NGs) consisting chitosan (CS) and carboxymethyl chitosan (CMCS) were successfully developed in our recent study [6]. The rational design of these nanocarriers was to retain the promising behavior of CS as an absorption enhancer [7,8], yet expand the range of absorption enhancement from limited duodenal segment to the entire small intestine. However, the behavior of CS/CMCS-NGs toward the intestinal barrier and different cellular and molecular interactions with intestine epithelium remain to be clarified.

Caco-2 cell model has been widely used to study the intestinal permeability of drugs. After differentiation, Caco-2 cells can form a monolayer of polarized cells which present tight junctions and active transporters (P-glycoprotein) [5]. Several studies using Caco-2 cells model or animal models have shown the uptake of CS-based NGs by Payer's patches [9] and the epithelium [10] as well. The endocytosis of CS-based NGs by Caco-2 cells was saturable, energy- and temperature-dependent, which indicated that this process might be an active transport [10]. However, the endocytosis approach of CS-based NGs especially for CS/CMCS-NGs is poorly characterized [22]. On the other hand, CS-based NGs have ability to open tight junctions (TJs) between intestinal epithelium and facilitate paracellular transport of drugs [11–14]. This capacity depends on the positive charge of CS under weak acidic condition, which is infeasible in intestinal segments other than duodenum [15,16]. But for CS/CMCS-NGs, the introduction of CMCS could maintain continues and efficient absorption enhancement of DOX throughout the

* Corresponding authors. College of Marine Life Science, Ocean University of China, Yushan Road, Qingdao 266003, Shandong Province, China. Tel./fax: +86 0532 82032586.
E-mail addresses: kongming@ouc.edu.cn (M. Kong), xgchen@ouc.edu.cn (X. Chen).
[1] These authors contributed equally to this manuscript as co-corresponding authors.

0939-6411/$ - see front matter © 2013 Elsevier B.V. All rights reserved.
http://dx.doi.org/10.1016/j.ejpb.2013.11.007

entire small intestine [6]. The mechanism of this phenomenon is still not clear yet.

This study was to investigate the mechanism regarding the transport of CS/CMCS-NGs throughout the intestinal barrier, particularly focused on the cellular and molecular mechanisms. Two possible routes have been studied by using well defined Caco-2 cell model. As for the transcellular pathway, different endocytosis mechanisms, including macropinocytosis, clathrin-, caveolae- and clathrin-independent mediated endocytosis have been studied in the presence of different inhibitors of protein-mediated endocytosis [17]. On the other hand, the transport of nanogels by paracellular pathways focused on the mechanism that CS/CMCS-NGs enhance intestinal absorption of anticancer drugs throughout the entire small intestine. Finally, the transport mechanism of this nanocarrier was evaluated *ex vivo* and *in vivo* using animal models and confirmed the findings of *in vitro* studies.

2. Materials and methods

2.1. Materials

CS (molecular weight, MW: 10 kDa, degree of deacetylation, DD: 89%) was obtained from Biotech Co. (Mokpo, Korea). CMCS (MW: 12 kDa, DD: 81%, Degree of substitution, DS: 92%) was synthesized and characterized by the method described by Chen [18]. Cy3-SE (Cy3-N-hydroxy-succinimide ester), fluorescein isothiocyanate (FITC), acetic acid and sodium triphosphate (TPP) were purchased from Sigma (St. Louis, USA). DOX was supplied by Zhejiang Hai zheng Co. Ltd. (China). All other reagents and solvents were of analytical grade.

2.2. Preparation of Cy3-CS and FITC-CMCS

Cy3-labeled chitosan (Cy3-CS) and FITC-labeled carboxymethyl chitosan (FITC-CMCS) were synthesized according to the methods described in the literature [19,20].

The synthesis of Cy3-CS was based on the reaction between the free amines on the chitosan and N-hydroxy-succinimide on Cy3–SE. A solution of Cy3–SE in DMSO (1 mg/mL) was prepared and added gradually to soluble chitosan (1 mg/mL, pH 6.6) with continuous stirring for 12 h in the dark.

The synthesis of FITC-CMCS was based on the reaction between the amine groups of O-CMCS and the isothiocyanate group of FITC. Briefly, CMCS (30 mg) was dissolved in water (15 mL) in a weakly acidic condition with 1 M HCl, and the pH was adjusted to 6.9 with 1 M NaOH. FITC (2.1 mg) was added, and the mixture was stirred at room temperature for 24 h.

After reaction, Cy3-CS and FITC-CMCS were dialyzed in tri-distilled water for 3 days to remove unreacted Cy3 or FITC. The products were precipitated with ethanol and then freeze-dried.

2.3. Preparation and characterization of DOX:CS/CMCS-NGs

DOX-loaded CS/CMCS-NGs (DOX:CS/CMCS-NGs) were prepared according to a modified process originally based on our previous work [6]. Briefly, DOX aqueous solution (1 mg/mL, 1 mL) was premixed with CMCS (1 mg/mL, 4 mL) under magnetic stirring for 30 min. Subsequently, CS solution (1 mg/mL, 3 mL, pH 6.6) and TPP (0.25 mg/mL, 2 mL) were blended with the mixture under constant stirring for 1 h, and nanogels formed.

The size distribution and zeta potential of the prepared DOX:CS/CMCS-NGs at pH 1.2, 2.5 (HCl), pH 6.6, 7.0, 7.4 (phosphate-buffered saline, PBS) were measured with a Zetasizer ZEN 3600 Nano Series apparatus (ZEN, UK).

The morphology of the prepared NGs was examined by scanning electron microscopy (SEM, JSM-6010LA, JEOL Ltd., Japan) and transmission electron microscope (TEM, JEM-1200EX, JEOL Ltd., Japan) at pH values 1.2, 6.6, 7.0 and 7.4, simulating environments of the gastric acid, duodenum, ileum or intercellular spaces of enterocytes, respectively.

The obtained DOX:CS/CMCS-NGs were washed with deionized water 3 times to remove the DOX onto the surface of the particles, collected via ultracentrifugation at 12,000 rpm for 30 min, and then freeze-dried for 48 h. To determine the loading efficiency (*LE*) and loading content (*LC*) of DOX in nanogels, the free DOX in supernatants was filtered through a membrane filter (0.45 μm), whose concentration was examined spectrophotometrically at 481 nm (UV-1100, Shimadzu Ltd., Japan). The *LE* and *LC* were calculated using Eqs. (1) and (2), respectively:

$$LE\ (\%) = \left(Does_{added} - Does_{free}\right)/Does_{added} * 100\ \% \quad (1)$$

$$LC\ (\%) = \left(Does_{added} - Does_{free}\right)/W_{nanogels} * 100\ \% \quad (2)$$

where $Does_{added}$ is total amount of DOX added, $Does_{free}$ is free DOX in solution, and $W_{nanogels}$ is weight of nanogels

2.4. Cytotoxicity studies

The human colon adenocarcinoma (Caco-2) cell line obtained by the American Type Culture Collection (Manassas, USA, between 25 and 35 passages) was utilized to evaluate the cytotoxicity of blank-NGs (CS/CMCS-NGs). The cells were cultured in DMEM (high glucose) and supplemented with 10% (v/v) fetal bovine serum and penicillin/streptomycin at 37 °C and maintained in a saturated humidity containing 5% CO_2. Briefly, cells (3×10^4 cells/mL) were seeded in 96-well culture plates. Various concentrations (0–1000 μg/mL) of CS/CMCS-NGs in cell culture medium were incubated for 24, 48, or 72 h followed by MTT assay. Meanwhile, the cytotoxicity of CS/CMCS-NGs (200 μg/mL) at different pH values (6.6, 7.0 and 7.4) was also tested after 24 h of incubation time with Caco-2 cells.

2.5. Transcellular transport

2.5.1. Passive or active transport

Biofluorescence NGs (Cy3-CS/FITC-CMCS-NGs) were prepared using Cy3-CS and FITC-CMCS as per the procedure described in Section 2.3 and used for fluorescence microscope or CLSM study. After 21 days of differentiation, the Caco-2 cells were incubated with Cy3-CS/FITC-CMCS-NGs (200 μg/mL, dissolved in Hank's Balanced Salt Solution, HBSS, pH 7.0) for 4 h in the dark at 4 °C or 37 °C. And then, the slides were washed in HBSS and nuclei were stained with 4′,6′-diamidino-2-phenylindolyl hydrochloride (DAPI, Sigma, 1 μg/mL) in HBSS [21]. Slides were then washed three times in HBSS and observed by fluorescence microscopy (Nikon Eclipse Ti-S, Nikon Ltd., Japan) and confocal laser scanning microscopy (CLSM, LSM510, Zeiss Ltd., Germany), respectively.

2.5.2. Characterization of DOX:CS/CMCS-NGs endocytosis

In order to identify the approach of transcellular transport used by DOX:CS/CMCS-NGs, transport experiments were performed in the presence of specific inhibitor for different types of endocytosis. Caco-2 cell were cultured on the tissue-culture-treated polycarbonate filters (diameter 24.5 mm, growth area 4.7 cm^2) in Costar Transwell 6 wells/plates (Corning Costar Corp., Corning, NY) 24–30 days after seeding (Transepithelial electrical resistance [TEER] values in the range of 600–800 $\Omega\,cm^2$) to form Caco-2 cell monolayer. Firstly, the cell monolayer was incubated with the medium containing the specific inhibitor for 1 h at 37 °C. Then, the transport experiment was performed in the presence of

Please cite this article in press as: C. Feng et al., Transport mechanism of doxorubicin loaded chitosan based nanogels across intestinal epithelium, Eur. J. Pharm. Biopharm. (2013), http://dx.doi.org/10.1016/j.ejpb.2013.11.007

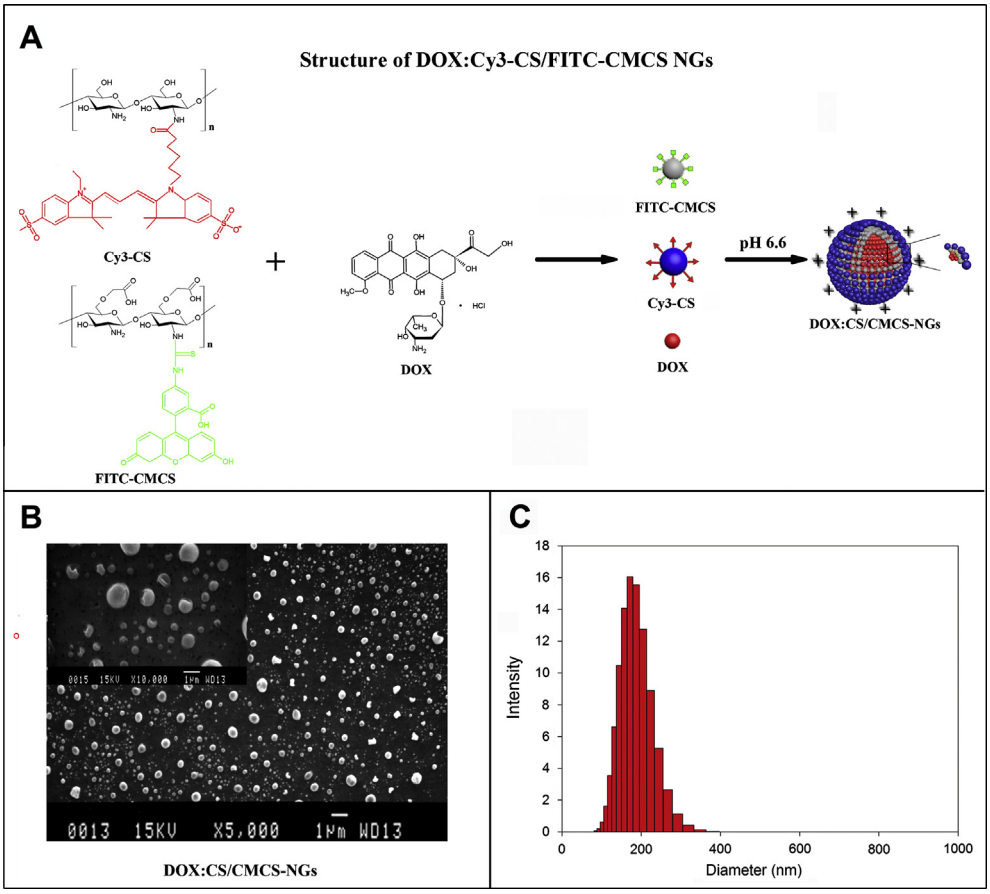

Fig. 1. (A) Structure of biofluorescence nanogels (DOX:Cy3-CS/FITC-CMCS-NGs). (B) SEM image of the nano-suspensions at pH 6.6 (the condition that test nanogels were prepared). (C) Hydrodynamic diameters and distributions of DOX:CS/CMCS-NGs (1 mg/mL) measured by dynamic light scattering in PBS buffer (pH 6.6) . (For interpretation of the references to colour in this figure legend, the reader is referred to the web version of this article.)

Table 1
Mean particle sizes and zeta potential values of DOX:CS/CMCS-NGs at distinct pH environments ($n = 5$).

pH value	Mean particle size (nm)	Zeta potential (mV)	PDI
1.2	197.2 ± 11.2	37.6 ± 0.8	0.235
2.5	258.7 ± 9.3	21.2 ± 1.7	0.132
6.6	279.3 ± 8.3	32.6 ± 1.1	0.155
7.0	442.2 ± 6.7	12.2 ± 0.6	0.635
7.4	▲	▲	▲

▲: Precipitation of aggregates was observed.

different inhibitors and 200 μg/mL DOX:CS/CMCS-NGs in the dark for 2 h at 37 °C. Control experiment was performed with HBSS for first incubation of cells. The inhibitors were as follows:

The inhibitor of macropinocytosis [17]: 30 μM m of Amiloride.
The inhibitor of caveola-mediated endocytosis [22,23]: 1 μg/mL of filipin.
The inhibitor of clathrin-mediated endocytosis [22,24]: 10 μg/mL of chlorpromazine.

The quantitative study was investigated according to previous report [3,25]. Briefly, after 2 h of incubation, samples were taken from apical and basolateral sides and DOX content was determined by HPLC. The detector was operated at a wavelength of 254 nm. Agilent Zorbax SB-C18 column (5 μm, 4.6 mm 250 mm) was used. Mobile phase consists of 50% acetate buffer (pH 5), 30% methanol and 20% acetonitrile. The flow rate was maintained at 1 mL/min.

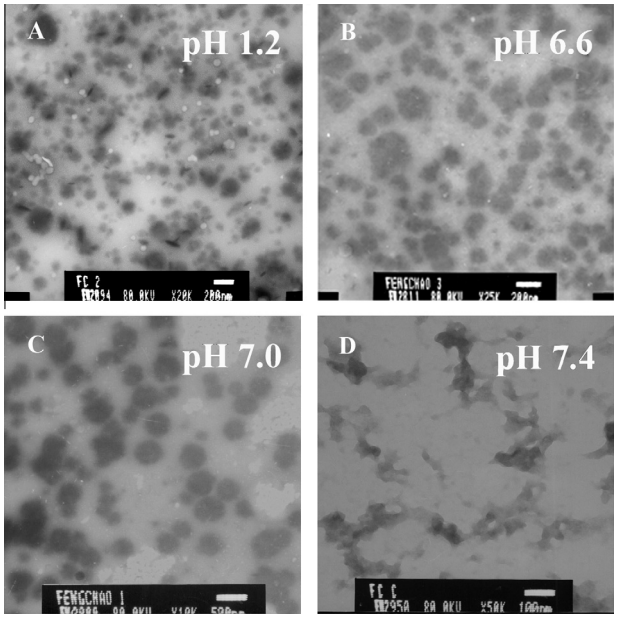

Fig. 2. TEM images of DOX:CS/CMCS-NGs at distinct pH values simulating GI tract (A: pH 1.2 simulating the stomach environment; B: pH 6.6 simulating the duodenum environment; C: pH 7.0 simulating the proximal ileum; D: pH 7.4 simulating the intercellular matrix of enterocytes).

Please cite this article in press as: C. Feng et al., Transport mechanism of doxorubicin loaded chitosan based nanogels across intestinal epithelium, Eur. J. Pharm. Biopharm. (2013), http://dx.doi.org/10.1016/j.ejpb.2013.11.007

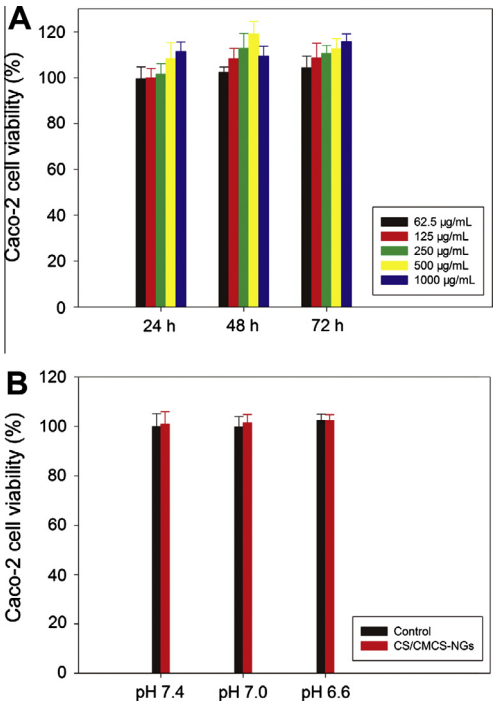

Fig. 3. *In vitro* cytotoxicity of CS/CMCS-NGs on Caco-2 cells: (A) Different incubation time of the cells with NGs at different concentrations. (B) Different pH environments. Data represent the mean ± SD ($n = 6$). (For interpretation of the references to colour in this figure legend, the reader is referred to the web version of this article.)

Apparent permeability coefficient (P_{app}) was calculated using Eq. (3):

$$P_{app} = Q/Act \tag{3}$$

where Q is the total amount of DOX permeated (ng), A is the surface area of monolayer (cm^2), c is the initial concentration of DOX over the apical side (μg/mL) and t is the time of the experiment (s).

Moreover, after collection of media, the bottom of the filter was absorbed onto paper in order to eliminate any basolateral medium, and cell monolayers were washed twice with ice-cold PBS (pH 7.4). Then, 0.5% Triton X-100 in 0.2 M NaOH solution was added to lyse the cells, and immediately frozen at −20 °C until analyzed by HPLC.

2.6. Paracellular transport

2.6.1. Capacity to bind Ca^{2+} of CS/CMCS-NGs

The capability of CS, CMCS and CS/CMCS-NGs for Ca^{2+} binding was respectively investigated according to the reported method [27] with some modifications. Briefly, 2 mg of the sample was placed in 4 mL of 0.0025 mmol/L $CaCl_2$ solution at different pH environments (pH 1.2 [0.1 N HCl], pH 6.6, 7.0, 7.4 [10 mM PBS]) for 24 h and then, ultracentrifuged 12,000 rpm. The supernatant was measured for free calcium by complexometric titration with Titriplex® III, using calcein as an indicator. The sample was then washed three times with corresponding buffer to take out the previously entrapped calcium (unbound Ca^{2+}), which was also measured by complexometric titration. The calcium binding capacity (BC) was thereby calculated using Eq. (4):

$$BC = \left(Ca^{2+}_{added} - Ca^{2+}_{free}\right)/W_{sample} \tag{4}$$

where Ca^{2+}_{added} is total amount of Ca^{2+} added (mmol), Ca^{2+}_{free} is unbound Ca^{2+} (mmol), and W_{sample} (g) is weight of sample.

2.6.2. TEER measurement

The grown cell monolayers (TEER values in the range of 600–800 Ω cm^2) were incubated with DOX (0.3% w/v, 0.5 mL, HBSS, pH 7.0); CS (0.3% w/v, 0.5 mL, HBSS, pH was adjusted by HCl to 6.6, 7.0 or 7.4); CMCS (0.3% w/v, 0.5 mL, HBSS, pH was adjusted by HCl to 6.6, 7.0 or 7.4); DOX:CS/CMCS-NGs (0.5 mg/mL, HBSS, pH was adjusted by HCl to 6.6, 7.0 or 7.4); DOX:CS/CMCS-NGs (0.5 mg/mL) + $CaCl_2$ (0.1 mg/mL) (HBSS, pH was adjusted by HCl to 6.6, 7.0 or 7.4). The TEER for the tightness of cell monolayers (or their paracellular permeability) was evaluated with a Millicell-Electrical Resistance System (Millipore Corp., Bedford, MA).

2.6.3. Transport of DOX across Caco-2 cells monolayers

One milliliter of transport medium (pH 7.0) containing DOX (0.5 mg/mL), DOX:CS/CMCS-NGs (equivalent to 0.5 mg/mL of DOX) or DOX:CS/CMCS-NGs (equivalent to 0.5 mg/mL of DOX) + $CaCl_2$ (0.1 mg/mL) was introduced into the donor compartment of the Caco-2 cell monolayers, while the medium in the receiver compartment was maintained at pH 7.4. Following incubation for 1 h at 37 °C, test samples were aspirated. Cells were then washed twice with pre-warmed PBS before they were fixed in 3.7% paraformaldehyde. Then, the fixed cells were observed by CLSM.

2.7. Animal study

2.7.1. Animals

Adult male Sprague–Dawley (SD) rats (220–250 g) were housed and cared in air-conditioned quarters under a photoperiod schedule of 12 h light/12 h dark cycles. The rats received standard laboratory chow and tap water available ad libitum 3 weeks prior to the experiments. All experiments on animals were carried out in accordance with the European Community Council Directive of November 24, 1986 (86/609/EEC).

2.7.2. Mucoadhesion and permeation enhancement

The mucoadhesion and absorption enhancement of Cy3-CS/FITC-CMCS-NGs in different segments of the small intestine (duodenum, jejunum and ileum) were studied via CLSM. The study was performed in a rat model ($n = 3$) using an in situ closed-loop technique. Overnight-fasted rats were anaesthetized via the intramuscular injection of chloralic hydras (10%, 0.004 mL/g, Sigma, St. Louis, USA). The abdominal cavity of animal was opened by a midline incision, and the small intestine was exposed. Different segments of the small intestine were identified based on their anatomical positions with respect to the stomach and the colon. A 5 cm section of each segment of the small intestine was selected for producing the closed-loop; the proximal end of each intestinal section was tied up before introducing Cy3-CS/FITC-CMCS-NGs (1 mg/mL, 0.5 mL) via a syringe. The distal end was then ligated to form a closed-loop. Rats were sacrificed 2 h later, and the closed-loop segments were dissected. Next, the dissected intestinal segments were washed with phosphate-buffered saline, fixed in 4% paraformaldehyde, processed for freezing microtomy and observed by CLSM.

2.7.3. In vivo and ex vivo biodistribution

Overnight-Fasted SD rats (hair removal by depilatory) were used in the biodistribution study refer to [28]. DOX:CS/CMCS-NGs or DOX:CS/CMCS-NGs with 20 mg/kg of $CaCl_2$ dissolved in saline were orally administrated at a dose of 5 mg DOX-equiv./kg body weight to investigate the effect of Ca^{2+} on NGs-induced absorption enhancement. The rats were anesthetized with injecting 10% chloral hydrate (0.004 mL/g); then, fluorescence images were obtained by small animal *in vivo* imaging instrument (Fusion FX7, Vilber Lourmat, France) at specific time intervals (0 h

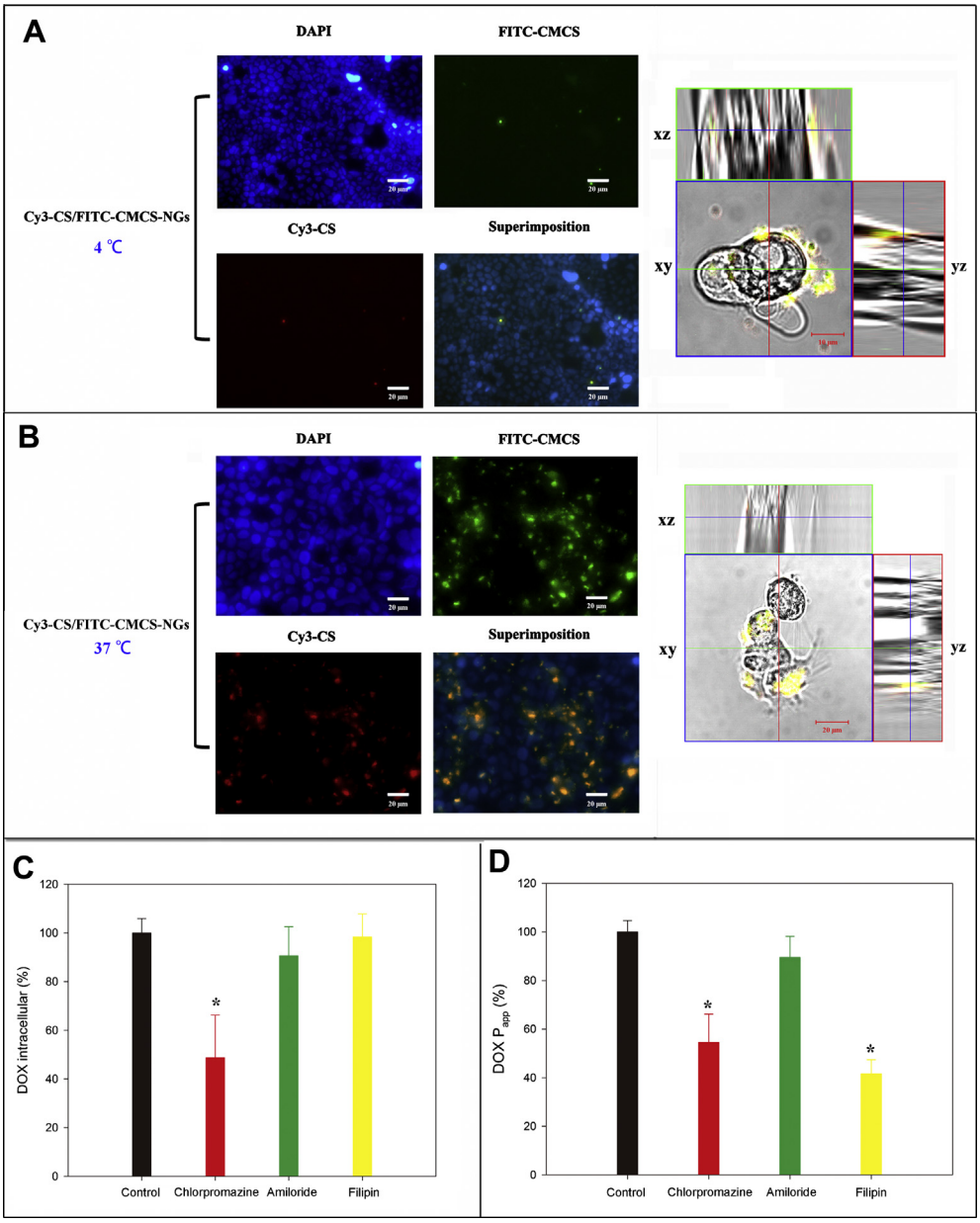

Fig. 4. Transcellular transport of DOX by CS/CMCS-NGs: fluorescence microscope and orthogonal views of CLSM images showing the uptake of Cy3-CS/FITC-CMCS-NGs in Caco-2 cells after 4 h incubition time at (A) 4 °C and (B) 37 °C. Variation of intracellular uptake and apparent permeability coefficients of DOX at 37 °C after 1 h of incubation with DOX:CS/CMCS-NGs and different endocytosis inhibitors: (C) Intracellular quantities of DOX (%), DOX:CS/CMCS-NGs without inhibitor were considered as 100 % of DOX intracellular. (D) P_{app} of (%) DOX, P_{app} of DOX:CS/CMCS-NGs without inhibitor was considered as 100 % of P_{app}; Data represent the mean ± SD, "*": vs. control; $p < 0.05$ ($n = 6$). (For interpretation of the references to colour in this figure legend, the reader is referred to the web version of this article.)

[untreated], 2 h, 4 h and 8 h). Filter sets (blue: excitation, 500–720 nm; exposure time, 300 ms and red: excitation, 670–900 nm; exposure time, 150 ms) were used to detect DOX-related fluorescence. At 10 h after administration orally, major organs (intestine, stomach, heart, liver, spleen, lung, and kidneys) were dissected from SD rats' bodies, then, observed by small animal *in vivo* imaging instrument. To determine DOX level in organs, tissues (0.5 g) were homogenized in 3 mL PBS (pH 7.4) using tissue homogenizer at 20,000 rpm for 5 min, then quantified with spectrofluorimetry at Ex/Em 537/584 nm.

2.7.4. Oral bioavailability

SD rats were used and randomly divided into two groups ($n = 5$ for each studied group). After fasting overnight, different formulations (DOX:CS/CMCS-NGs solution [10 mg DOX-equiv./kg body weight, 1 mL] or DOX:CS/CMCS-NGs [10 mg DOX-equiv./kg body weight, 1 mL] with 20 mg/kg of $CaCl_2$) were administered orally to the rats. Blood samples were collected from the tails of rats at particular time intervals after administration of each formulation in micro-centrifuge tubes containing 20 μL of EDTA solution. Plasma was collected by centrifuging the blood samples at 5000 rpm for 10 min at 25 °C. Acetonitrile (0.2 mL) was added in plasma (0.2 mL) vortexed vigorously for 2 min and then centrifuged at 15,000 rpm for 15 min at 25 °C. Then, the supernatant was analyzed by HPLC. The relative bioavailability was calculated as Eq. (5):

$$Relative\ bioavailability\ (\%) = \left(AUC_{NGs}/AUC_{NGs/Ca}\right) * \left(Does_{NGs/Ca}/Does_{NGs}\right) * 100\ \% \quad (5)$$

Please cite this article in press as: C. Feng et al., Transport mechanism of doxorubicin loaded chitosan based nanogels across intestinal epithelium, Eur. J. Pharm. Biopharm. (2013), http://dx.doi.org/10.1016/j.ejpb.2013.11.007

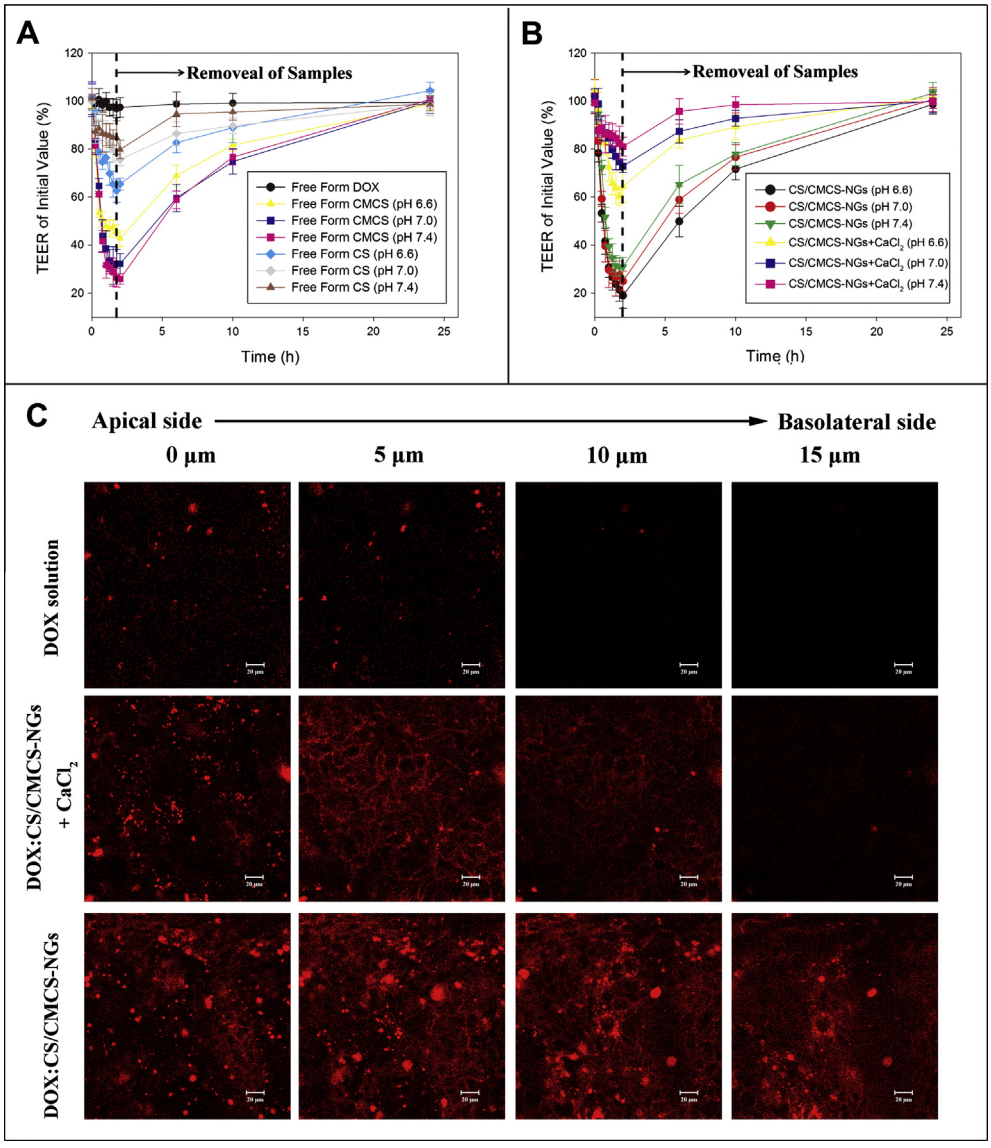

Fig. 6. Paracellular transport of DOX by CS/CMCS-NGs: (A) Effects of DOX, CMCS and CS on the transepithelial electrical resistance (TEER) of Caco-2 cell monolayers at different pH environments. (B) Effects of DOX:CS/CMCS-NGs and DOX:CS/CMCS-NGs + $CaCl_2$ on the TEER of Caco-2 cell monolayers at different pH environments. (C) CLSM images of 4 optical sections of the transport of DOX across Caco-2 cell monolayers. (For interpretation of the references to colour in this figure legend, the reader is referred to the web version of this article.)

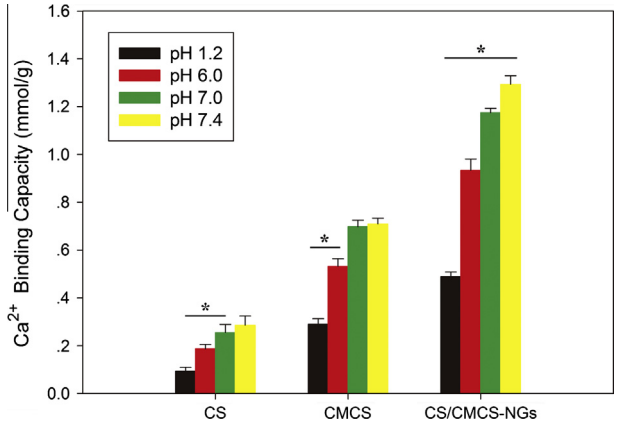

Fig. 5. Ca^{2+} binding capability of CS, CMCS and CS/CMCS-NGs at distinct pH environments, "*": $p < 0.05$ ($n = 4$). (For interpretation of the references to colour in this figure legend, the reader is referred to the web version of this article.)

where *AUC* is the area above the baseline curve calculated from zero time to 24 h. The subscript *NGs* and *NGs/Ca* refer to group of rats orally given DOX:CS/CMCS-NGs and DOX:CS/CMCS-NGs + $CaCl_2$ solution, respectively.

2.8. Statistical analysis

The assays were performed at least in triplicate on separate occasions. Statistical analysis of the differences in the measured properties of the groups was performed with one way analysis of variance and the determination of confidence intervals with the statistical package Sigma Plot, version 11.0 (Systat Software Inc., US). The data collected in this study were expressed as means and standard deviations, indicated as "mean ± SD." Differences were considered to be statistically significant when the p values were less than 0.05.

Please cite this article in press as: C. Feng et al., Transport mechanism of doxorubicin loaded chitosan based nanogels across intestinal epithelium, Eur. J. Pharm. Biopharm. (2013), http://dx.doi.org/10.1016/j.ejpb.2013.11.007

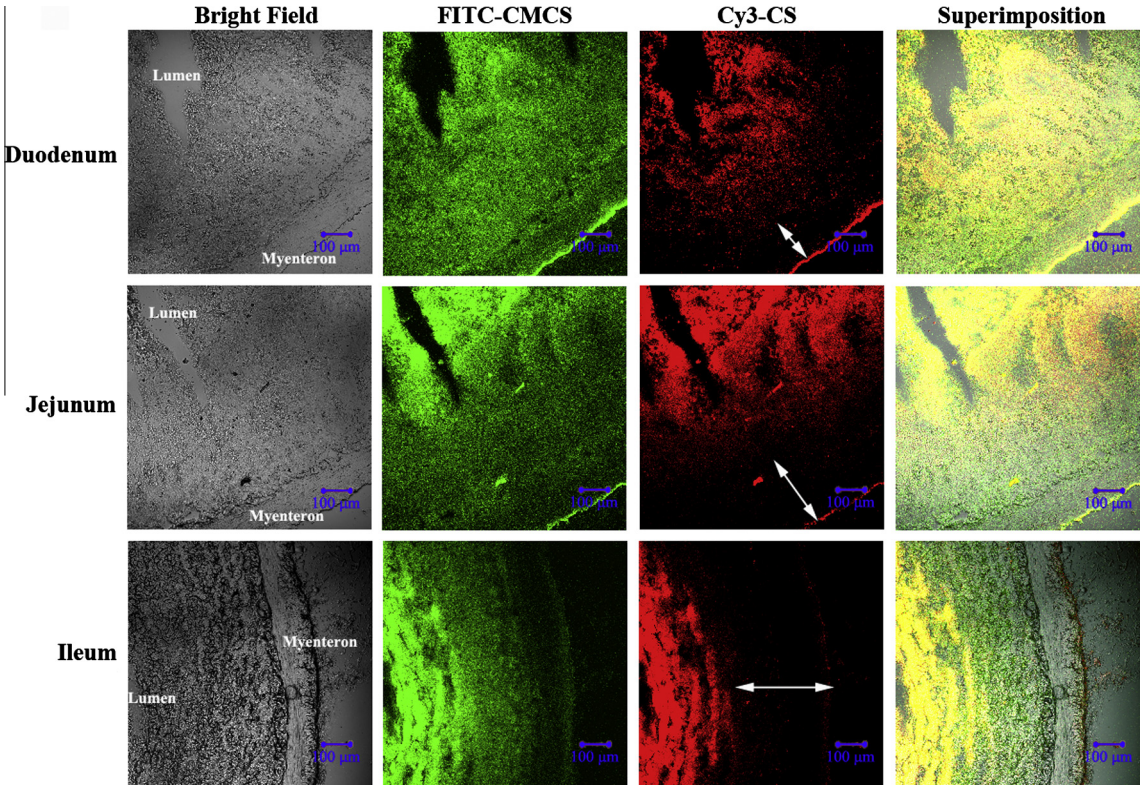

Fig. 7. CLSM images showing the mucoadhesion and the absorption of Cy3-CS/FITC-CMCS-NGs (FITC-CMCS, green; Cy3-CS, red) in different segments of the small intestine. (For interpretation of the references to colour in this figure legend, the reader is referred to the web version of this article.)

3. Results and discussion

3.1. Development and characterization of DOX:CS/CMCS-NGs

DOX:CS/CMCS-NGs were prepared by ionic gelation in the presence of TPP. The obtained nanogels were typically spherical and capsular (Fig. 1B). The diameter of DOX:CS/CMCS-NGs was 279.3 ± 8.3 nm with narrow size distribution (Fig. 1C, Table 1, pH 6.6: prepared pH condition, polydispersity index: PDI $\leqslant$ 0.2) and zeta potential was about 30 mV (Table 1, pH 6.6). In an aqueous environment (pH 6.6), electrostatic interaction occurred between the anionic CMCS ($-COO^-$) and the cationic CS ($-NH^{3+}$), facilitating the encapsulation of DOX in NGs. (Fig. 1A). The *LE* and *LC* of DOX were 71.85 ± 3.1 and 20.3 ± 0.5.

The stability of DOX:CS/CMCS-NGs was investigated in different pH environments simulating GI tract (pH 1.2: stomach, pH 6.6: duodenum, pH 7.0: proximal ileum, pH 7.4: intercellular matrix of enterocytes environment). The pK_a values of CS and TPP are 6.5 and 1.0–2.1, respectively. O-carboxymethyl chitosan (CMCS) was an amphoteric polyelectrolyte whose isoelectric point was about 4. At pH 1.2, the amino groups on CS and CMCS were protonized; the phosphate groups on TPP were ionized. Therefore, positively charged CMCS, CS and negatively charged TPP were able to form polyelectrolyte complexes via electrostatic interaction, giving rise to spherical shape (Fig. 2A) and narrow size distribution (PDI: 0.235 [pH 1.2], Table 1). At pH 6.6, the most amino groups on CS and CMCS were still protonized and the carboxyl groups on CMCS were ionized, thus the polyelectrolyte complexes were stable due to the strong electrostatic interaction among positively charged CS and negatively charged CMCS, TPP (Fig. 2B). At pH 7.0, some of the $-NH_3^+$ on CS had partially became deprotonized, consequently weakening the electrostatic interaction between CS, CMCS and TPP, but the negative charged CMCS was still able to maintain the stability of polyelectrolyte complexes (Fig. 2C). The NGs were swollen and its particle size was 442.2 ± 6.7 nm (Table 1), which was significantly larger than that in acid condition. Similarly, at pH 7.4, CS were further deprotonized, resulting in the mass structure loose completely and the NGs became disintegrated and precipitated (Fig. 2D). These results indicated the DOX:CS/CMCS-NGs were tolerant to low pH condition and stable in GI tract.

3.2. Cytotoxicity studies

The cytotoxicity of blank-NGs (CS/CMCS-NGs) was tested with Caco-2 cells at different concentrations of CS/CMCS-NGs and culture time. The viabilities of Caco-2 cells were above 105% at all concentrations during 72 h tested (Fig. 3A). Meanwhile, blank-NGs (200 μg/mL) exhibited no cytotoxicity for Caco-2 cells at different pH values (pH 6.6, 7.0 and 7.4, Fig. 3B, $p > 0.05$ vs. control).

3.3. Transcellular transport

3.3.1. Passive or active transport

The uptake of Cy3-CS/FITC-CMCS-NPs by Caco-2 cells with incubation time of 4 h was visualized using fluorescence microscope and CLSM. The overlap of red (Cy3-CS) and green (FITC-CMCS) fluorescence appeared yellow signal that indicated integrity of the NGs. No apparent fluorescence was detected in Caco-2 cells incubated with Cy3-CS/FITC-CMCS-NGs at 4 °C (Fig. 4A). Orthogonal views of CLSM images showed that the NGs located just on the cell membrane but failed to enter into cells. This phenomenon manifested that the uptake of Cy3-CS/FITC-CMCS-NGs by Caco-2 cell was not a passive process because the cell membrane penetration at 4 °C was more related to passive processes, such as modification of membrane fluidity, instead of active processes [26,28,29]. At 37 °C, Cy3-CS/FITC-CMCS-NGs were found to be distributed inside of the

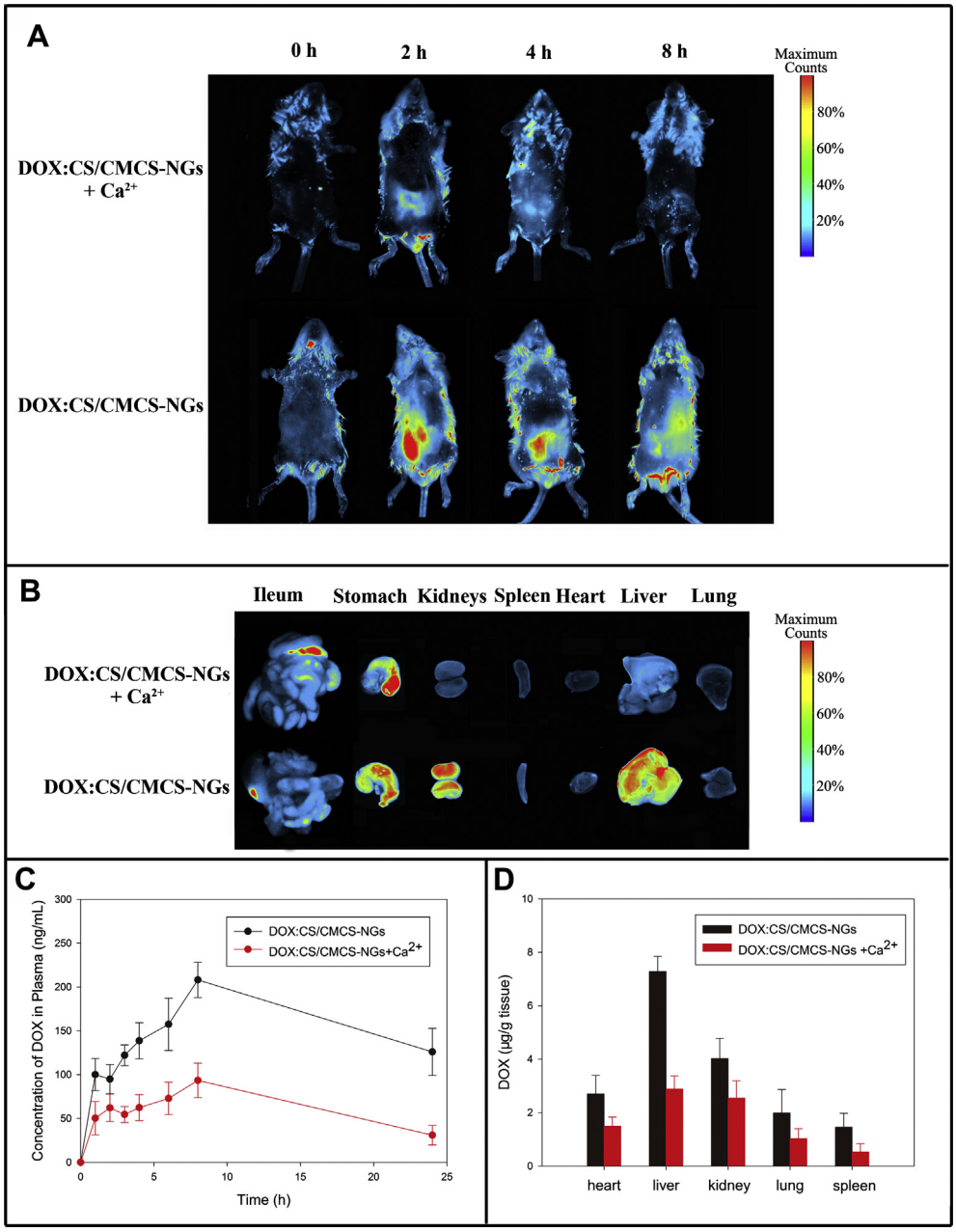

Fig. 8. (A) *In vivo* noninvasive flourescence imaging DOX distribution in rats. (B) *Ex vivo* fluorescence imaging of organs at 10 h post-oral-administration. (C) DOX plasma concentration vs. time profiles of oral administration. (D) Quantification of tissue distribution of DOX in rats ($n = 5$). (For interpretation of the references to colour in this figure legend, the reader is referred to the web version of this article.)

Caco-2 cells as yellow fluorescent spot (Fig. 4B). Orthogonal views of CLSM images clearly exhibited the localization of NGs in cells. These results demonstrated that the CS/CMCS-NGs could be likely internalized by an active uptake or transported across Caco-2 cells, which was similar to chitosan-coated lipid nanoparticles [29] and chitosan-PLGA nanoparticles [30,31].

3.3.2. Characterization of NGs endocytosis

To figure out what endocytosis mechanism that CS/CMCS-NGs were uptaken by Caco-2 cells, the transport experiments were performed in the presence of amiloride (inhibitor of macropinocytosis), chlorpromazine (inhibitor of clathrin-mediated endocytosis) and filipin (inhibitor of caveola-mediated endocytosis), respectively. Intracellular DOX concentration was determined by HPLC after cell lysis and DOX concentration on the apical and basolateral sides was also determined to calculate the apparent permeability coefficient. The cellular uptake of DOX was not affected by the presence of filipin and amiloride ($p > 0.05$ vs. control), but it was significantly inhibited by co-administered chlorpromazine (Fig. 4C). The intracellular concentration of DOX was found to decrease by 52.32%, suggesting that clathrin-mediated endocytosis played important role in the internalization of the DOX:CS/CMCS-NGs. The incomplete inhibition of intracellular DOX content by 10 μg/mL of chlorpromazine demonstrated clathrin-independent pathways might also be involved. But caveolae-mediated pathway played marginal part because the DOX:CS/CMCS-NGs uptake was unaffected by co-administered 1 μg/mL of filipin. On the other hand, the transport results of DOX:CS/CMCS-NGs in the presence of different inhibitors have showed that a decrease in transport of DOX in the presence of chlorpromazine was observed again, but it

Please cite this article in press as: C. Feng et al., Transport mechanism of doxorubicin loaded chitosan based nanogels across intestinal epithelium, Eur. J. Pharm. Biopharm. (2013), http://dx.doi.org/10.1016/j.ejpb.2013.11.007

was less important than filipin (Fig. 4D). This phenomenon was inconsistent with earlier results (Fig. 4C), which could be attributed from the interference of cholesterol-binding agent (filipin) with the chitosan–membrane interaction by modifying the cell membrane properties [32], and thus inhibited the paracellular transport of DOX.

3.4. Paracellular transport

3.4.1. Capacity to bind Ca^{2+} of CS/CMCS-NGs

The cadherins at adherens junctions (AJs) are a group of Ca^{2+}-dependent adhesion molecules essential for the induction and maintenance of TJ assembly [15]. Chelation of Ca^{2+} disrupts TJ assembly and thus markedly enhances the paracellular permeability and attenuates the development of TEER. Therefore, the Ca^{2+} binding capacity of CS, CMCS and CMCS/CS-NGs was tested at different pH values simulating the GI tract environment (Fig. 5). The presence of $-COO^-$ group imparted CMCS with excellent Ca^{2+} binding capacity compared to CS ($p < 0.05$). And, the 3D structure of nanogel further strengthened this binding capacity which was at least 4-fold higher than that of CS at either pH value. These results demonstrated that CS/CMCS-NGs had a strong binding ability of Ca^{2+}. Most importantly, the chelation of CS/CMCS-NGs could be strengthened in the jejunum and ileum where pH value above 7.0.

3.4.2. TEER measurements

The variations in TEER of Caco-2 cell monolayers produced by the components of DOX:CS/CMCS-NGs (DOX, CS and CMCS) were respectively studied in different pH values stimulating GI tract. Compared with the group treated with DOX, the cell monolayers incubated with CS or CMCS displayed a transient and reversible decrease in TEER ($p < 0.05$, Fig. 6A). But, the extents in TEER reduction produced by CMCS were 1.7-fold at pH 6.6, 2.9-fold at pH 7.0 and 3.3-fold at pH 7.4 higher than that produced by CS at corresponding pH values, suggesting that CMCS was more effective as an absorption enhancer than CS, especially at neutral pH values (Fig. 6A). This phenomenon was corresponding to their respective *in vitro* affinities for Ca^{2+}.

To further illustrate the effect of Ca^{2+} on NGs-induced paracellular transport enhancement, the Caco-2 cell monolayer was incubated with CS/CMCS-NGs or CS/CMCS-NGs + $CaCl_2$ (Fig. 6B). CS/CMCS-NGs group displayed a remarkable decrease in TEER, regardless of the pH environment exposed. But the introduction of Ca^{2+} obviously inhibited the extents of TEER reduction at either pH value. These results were attributed to the fact that the extra added Ca^{2+} weakened the chelating ability of CMCS and thus inhibited NGs-induced TJs opening.

3.4.3. Transport of DOX by Caco-2 cell monolayers

The transport of DOX or those released from DOX:CS/CMCS-NGs across Caco-2 cell monolayers was visualized using CLSM. At 2 h after the incubation with free DOX, no apparent fluorescence signal was observed in the paracellular pathway (Fig. 6C). In contrast, red fluorescent was clearly observed at intercellular spaces between adjacent cells, suggesting paracellular permeation of DOX through cell monolayers for DOS:CS/CMCS-NGs and DOX:CS/CMCS-NGs + $CaCl_2$ group. However, the fluorescent signal for cell monolayers incubated with DOX:CS/CMCS-NGs + $CaCl_2$ was weaker and appeared shallower than those of their counterparts that had been incubated with DOS:CS/CMCS-NGs. These findings supported the TEER measurements (Fig. 6B) and demonstrated that the higher

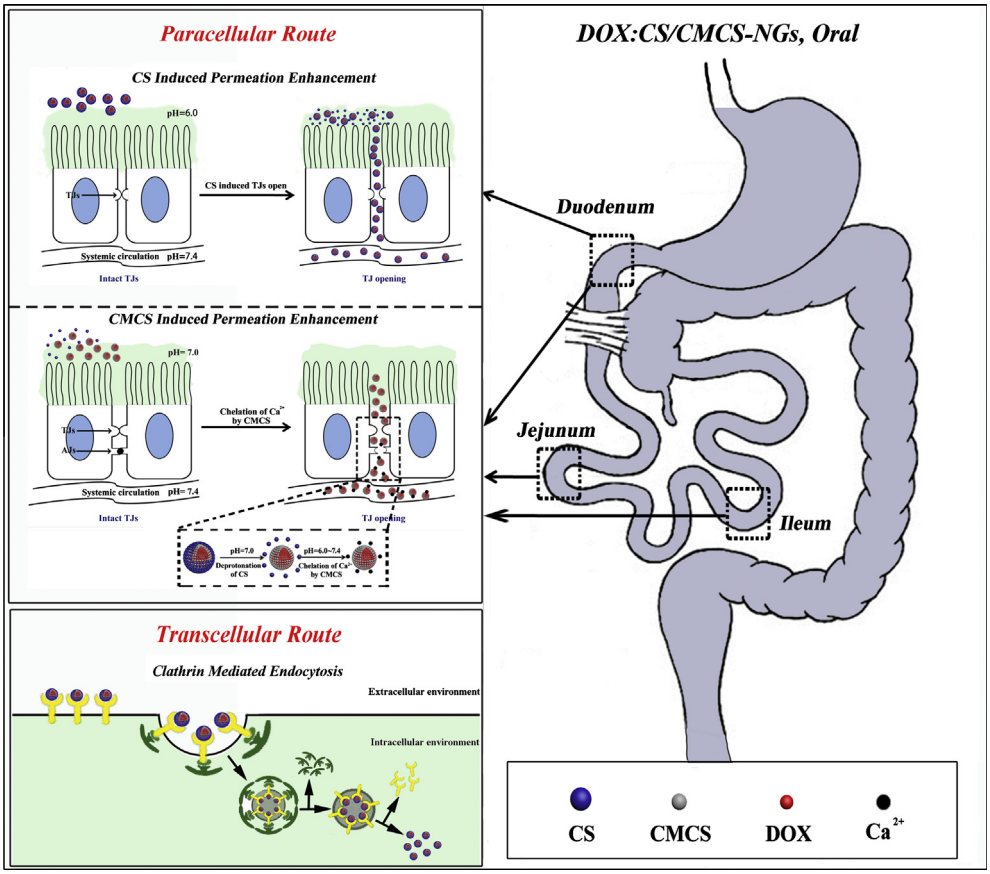

Fig. 9. Schematic diagrams displaying the transport mechanisms of DOX:CS/CMCS-NGs in small intestine.

Please cite this article in press as: C. Feng et al., Transport mechanism of doxorubicin loaded chitosan based nanogels across intestinal epithelium, Eur. J. Pharm. Biopharm. (2013), http://dx.doi.org/10.1016/j.ejpb.2013.11.007

capacity to binding Ca^{2+} of CS/CMCS-NGs was beneficial for paracellular transport of DOX.

3.5. Animal study

3.5.1. Mucoadhesion and permeation enhancement of CS/CMCS-NGs

The prolonged gastrointestinal transit offered by a mucoadhesive carrier system can increase the contact of the released drug with the underlying epithelium, and increased the drug absorption consequently [33]. The mucoadhesive and permeation ability of Cy3-CS/FITC-CMCS-NGs were examined in different segments of the small intestine via CLSM (Fig. 7). A great amount of CMCS in NGs (FITC-CMCS, green fluorescence) entered into the myenteron of small intestine. However, the permeation of CS in NGs (Cy3-CS, red fluorescence) into the myenteron of the jejunum (pH 7.0) and ileum (pH 7.4) was clearly poorer than the duodenum (pH 6.6) (Fig. 7, white double arrows). The protonated CS in NGs has excellent mucoadhesive ability, owing to its interaction with the negatively charged sialic-acid groups in mucin [34]. However, in intestinal segments other than duodenum, where environmental pH is above CS' pK_a (pH 6.5); deprotonation of CS would compromise the electrostatic interaction and the mucoadhesive ability. These results indicated that in the jejunum and ileum, the CMCS in NGs played a major role in mucoadhesion and permeation enhancement.

3.5.2. Biodistribution study

The biodistribution of DOX:CS/CMCS-NGs was investigated in rats (Sprague–Dawley, 220–250 g) and the fluorescent signal of DOX was detected by the small animal *in vivo* imaging instrument. To confirm the transport mechanism of DOX:CS/CMCS-NGs, high doses of the $CaCl_2$ were orally co-administrated with DOX:CS/CMCS-NGs to weaken their capacity to binding Ca^{2+}. Real-time images of DOX:CS/CMCS-NGs with or without the Ca^{2+} are presented in Fig. 8A. No apparent fluorescent signal was observed in the DOX:CS/CMCS-NGs with Ca^{2+} group during 8 h detection, This may be due to the weakened of capacity to binding Ca^{2+} of DOX:CS/CMCS-NGs being followed by a reduction in absorption DOX. On the contrary, fluorescent intensity of DOX in DOX:CS/CMCS-NGs without Ca^{2+} group was strong for the first 4 h and maintained for 8 h. Furthermore, the major organs were dissected at 10 h after oral administration and observed by *ex vivo* imaging (Fig. 8B). Fluorescent signal in DOX:CS/CMCS-NGs with Ca^{2+} group detected only in ileum and stomach. But for DOX:CS/CMCS-NGs without Ca^{2+} group, fluorescence signal was apparently rich in liver and kidneys, besides ileum and stomach. The results of quantitative experiment showed that all organs in DOX:CS/CMCS-NGs group exhibited significant higher DOX level than DOX:CS/CMCS-NGs with Ca^{2+} group (Fig. 8D). The liver exhibited the highest level (7.28 μg/g tissue), followed by kidneys (4.03 μg/g tissue), heart (2.70 μg/g tissue), lung (1.99 μg/g tissue), and spleen (1.46 μg/g tissue).

3.5.3. Oral bioavailability

Oral DOX:CS/CMCS-NGs could maintain 94.9–208.07 ng/mL of DOX in plasma during 24 h (Fig. 8C). The highest DOX concentration in the plasma was nearly 2.3-fold higher than that of oral DOX:CS/CMCS-NGs with $CaCl_2$ solution. And the relative bioavailability DOX:CS/CMCS-NGs was 248% compared to DOX:CS/CMCS-NGs with Ca^{2+}.

Above *in vivo* results confirmed that the enhanced DOX absorption was determined by the capacity to binding Ca^{2+} of CS/CMCS-NGs, which were consistent with the results of the *in vitro* transport studies.

3.6. Absorption enhancement mechanism of CS/CMCS-NGs

The aforementioned results indicated that the excellent DOX absorption assisted by CS/CMCS-NGs occurs by both paracellular and transcellular pathway (Fig. 9). The enhancing effect of CS and CMCS in NGs promoted paracellular permeation of DOX. In the duodenum (pH < 7), protonated CS in NGs enhanced paracelluar transport of DOX by TJs opening. Meanwhile, the CMCS in NGs deprived Ca^{2+} from AJs by favor of carboxylic groups and further promoted the TJs disruption. In the jejunum and ileum (pH $\geqslant$ 7), CS in NGs was deprotonated while the CMCS in NGs still could guarantee continuous and enhancing drug absorption. On the other hand, the clathrin-mediated and clathrin-independent endocytosis of DOX-CS/CMCS-NGs further strengthened the drug absorption by transcellular pathway.

4. Conclusions

CS/CMCS-NGs could markedly enhance paracellular transport of DOX throughout the entire small intestine by chelating Ca^{2+}. Meanwhile, DOX:CS/CMCS-NGs could be uptaken by Caco-2 cells mainly via active endocytosis particularly through clathrin-mediated pathway, which enhanced transcellular transport of DOX in small intestine. The high transport capacity of CS/CMCS-NGs by paracellular and transcellular pathway guaranteed the excellent absorption of encapsulated DOX throughout the entire small intestine.

Acknowledgments

This work was supported by National Natural Science Foundation of China (Nos. 81271727, 31240007), International Science Technology Cooperation Program of China (No. 2013DFG32880), Ph.D. Programs Foundation of Ministry of Education of China (No. 20120132110012) and Scholarship Award for Excellent Doctoral Student granted by Ministry of Education.

References

[1] K. Thanki, R.P. Gangwal, A.T. Sangamwar, S. Jain, Oral delivery of anticancer drugs: challenges and opportunities, J. Control. Release 170 (2013) 15–40.
[2] L. Mei, Z. Zhang, L. Zhao, L. Huang, X.L. Yang, J. Tang, S.S. Feng, Pharmaceutical nanotechnology for oral delivery of anticancer drugs, Adv. Drug Deliv. Rev. 65 (2013) 880–890.
[3] D.M. Benival, P.V. Devarajan, Lipomer of doxorubicin hydrochloride for enhanced oral bioavailability, Int. J. Pharm. 423 (2012) 554–561.
[4] A. Grenha, C. Remunan-Lopez, E.L. Carvalho, B. Seijo, Microspheres containing lipid/chitosan nanoparticles complexes for pulmonary delivery of therapeutic proteins, Eur. J. Pharm. Biopharm. 69 (2008) 83–93.
[5] L. Bromberg, V. Alakhov, Effects of polyether-modified poly(acrylic acid) microgels on doxorubicin transport in human intestinal epithelial Caco-2 cell layers, J. Control. Release 88 (2003) 11–22.
[6] C. Feng, Z.G. Wang, C.Q. Jiang, M. Kong, X. Zhou, Y. Li, X.J. Cheng, X.G. Chen, Chitosan/o-carboxymethyl chitosan nanoparticles for efficient and safe oral anticancer drug delivery: in vitro and in vivo evaluation, Int. J. Pharm. 457 (2013) 158–167.
[7] M.T. Cook, G. Tzortzis, V.V. Khutoryanskiy, D. Charalampopoulos, Layer-by-layer coating of alginate matrices with chitosan–alginate for the improved survival and targeted delivery of probiotic bacteria after oral administration, J. Mater. Chem. B 1 (2013) 52.
[8] A. Ahmed, J. Hearn, W. Abdelmagid, H. Zhang, Dual-tuned drug release by nanofibrous scaffolds of chitosan and mesoporous silica microspheres, J. Mater. Chem. 22 (2012) 25027–25035.
[9] O. Borges, A. Cordeiro-da-Silva, S.G. Romeijn, M. Amidi, A. de Sousa, G. Borchard, H.E. Junginger, Uptake studies in rat Peyer's patches, cytotoxicity and release studies of alginate coated chitosan nanoparticles for mucosal vaccination, J. Control. Release 114 (2006) 348–358.
[10] I. Behrens, A. Pena, M. Alonso, T. Kissel, Comparative uptake studies of bioadhesive and non-bioadhesive nanoparticles in human intestinal cell lines and rats: the effect of mucus on particle adsorption and transport, Pharm. Res. 19 (2002) 1185–1193.
[11] Y.H. Lin, K. Sonaje, K.M. Lin, J.H. Juang, F.L. Mi, H.W. Yang, H.W. Sung, Multi-ion-crosslinked nanoparticles with pH-responsive characteristics for oral delivery of protein drugs, J. Control. Release 132 (2008) 141–149.

[12] K. Sonaje, E.-Y. Chuang, K.-J. Lin, T.-C. Yen, F.-Y. Su, M.T. Tseng, H.-W. Sung, Opening of epithelial tight junctions and enhancement of paracellular permeation by chitosan: microscopic, ultrastructural, and computed-tomographic observations, Mol. Pharm. 9 (2012) 1271–1279.
[13] D. Teijeiro-Osorio, C. Remunan-Lopez, M.J. Alonso, Chitosan/cyclodextrin nanoparticles can efficiently transfect the airway epithelium in vitro, Eur. J. Pharm. Biopharm. 71 (2009) 257–263.
[14] T. Zou, S.S. Percival, Q. Cheng, Z. Li, C.A. Rowe, L. Gu, Preparation, characterization, and induction of cell apoptosis of cocoa procyanidins–gelatin–chitosan nanoparticles, Eur. J. Pharm. Biopharm. 82 (2012) 36–42.
[15] F.Y. Su, K.J. Lin, K. Sonaje, S.P. Wey, T.C. Yen, Y.C. Ho, N. Panda, E.Y. Chuang, B. Maiti, H.W. Sung, Protease inhibition and absorption enhancement by functional nanoparticles for effective oral insulin delivery, Biomaterials 33 (2012) 2801–2811.
[16] K. Sonaje, K.-J. Lin, M.T. Tseng, S.-P. Wey, F.-Y. Su, E.-Y. Chuang, C.-W. Hsu, C.-T. Chen, H.-W. Sung, Effects of chitosan-nanoparticle-mediated tight junction opening on the oral absorption of endotoxins, Biomaterials 32 (2011) 8712–8721.
[17] S.D. Conner, S.L. Schmid, Regulated portals of entry into the cell, Nature 422 (2003) 37–44.
[18] X.-G. Chen, H.-J. Park, Chemical characteristics of O-carboxymethyl chitosans related to the preparation conditions, Carbohyd. Polym. 53 (2003) 355–359.
[19] Y.P. Ho, H.H. Chen, K.W. Leong, T.H. Wang, Evaluating the intracellular stability and unpacking of DNA nanocomplexes by quantum dots-FRET, J. Control. Release 116 (2006) 83–89.
[20] L. Yin, L. Fei, F. Cui, C. Tang, C. Yin, Superporous hydrogels containing poly(acrylic acid-co-acrylamide)/O-carboxymethyl chitosan interpenetrating polymer networks, Biomaterials 28 (2007) 1258–1266.
[21] C.A. Schutz, L. Juillerat-Jeanneret, P. Kauper, C. Wandrey, Cell response to the exposure to chitosan-TPP//alginate nanogels, Biomacromolecules 12 (2011) 4153–4161.
[22] Z. Ma, L.-Y. Lim, Uptake of chitosan and associated insulin in Caco-2 cell monolayers: a comparison between chitosan molecules and chitosan nanoparticles, Pharm. Res. 20 (2003) 1812–1819.
[23] P.A. Orlandi, Filipin-dependent inhibition of cholera toxin: evidence for toxin internalization and activation through caveolae-like domains, J. Cell Biol. 141 (1998) 905–915.
[24] L.H. Wang, K.G. Rothberg, R.G. Anderson, Mis-assembly of clathrin lattices on endosomes reveals a regulatory switch for coated pit formation, J. Cell Biol. 123 (1993) 1107–1117.
[25] S. Ahmed, N. Kishikawa, K. Ohyama, M. Wada, K. Nakashima, N. Kuroda, Selective determination of doxorubicin and doxorubicinol in rat plasma by HPLC with photosensitization reaction followed by chemiluminescence detection, Talanta 78 (2009) 94–100.
[26] M.M. Canali, L.P. Pedrotti, J. Balsinde, C. Ibarra, S.G. Correa, Chitosan enhances transcellular permeability in human and rat intestine epithelium, Eur. J. Pharm. Biopharm. 80 (2012) 418–425.
[27] F.A. Dorkoosh, J.C. Verhoef, G. Borchard, M. Rafiee-Tehrani, H.E. Junginger, Development and characterization of a novel peroral peptide drug delivery system, J. Control. Release 71 (2001) 307–318.
[28] S. Zhu, M. Hong, L. Zhang, G. Tang, Y. Jiang, Y. Pei, PEGylated PAMAM dendrimer-doxorubicin conjugates: in vitro evaluation and in vivo tumor accumulation, Pharm. Res. 27 (2010) 161–174.
[29] F.M. Goycoolea, G. Lollo, C. Remunan-Lopez, F. Quaglia, M.J. Alonso, Chitosan–alginate blended nanoparticles as carriers for the transmucosal delivery of macromolecules, Biomacromolecules 10 (2009) 1736–1743.
[30] H. Sang Yoo, T. Gwan Park, Biodegradable nanoparticles containing protein-fatty acid complexes for oral delivery of salmon calcitonin, J. Pharm. Sci. 93 (2004) 488–495.
[31] S. Taetz, N. Nafee, J. Beisner, K. Piotrowska, C. Baldes, T.E. Murdter, H. Huwer, M. Schneider, U.F. Schaefer, U. Klotz, C.M. Lehr, The influence of chitosan content in cationic chitosan/PLGA nanoparticles on the delivery efficiency of antisense 2′-O-methyl-RNA directed against telomerase in lung cancer cells, Eur. J. Pharm. Biopharm. 72 (2009) 358–369.
[32] K.G. Rothberg, Y.S. Ying, B.A. Kamen, R.G. Anderson, Cholesterol controls the clustering of the glycophospholipid-anchored membrane receptor for 5-methyltetrahydrofolate, J. Cell Biol. 111 (1990) 2931–2938.
[33] L. Yin, J. Ding, C. He, L. Cui, C. Tang, C. Yin, Drug permeability and mucoadhesion properties of thiolated trimethyl chitosan nanoparticles in oral insulin delivery, Biomaterials 30 (2009) 5691–5700.
[34] I.A. Sogias, A.C. Williams, V.V. Khutoryanskiy, Why is chitosan mucoadhesive?, Biomacromolecules 9 (2008) 1837–1842

Please cite this article in press as: C. Feng et al., Transport mechanism of doxorubicin loaded chitosan based nanogels across intestinal epithelium, Eur. J. Pharm. Biopharm. (2013), http://dx.doi.org/10.1016/j.ejpb.2013.11.007